APSB
Acta Pharmaceutica Sinica B

CrossMark
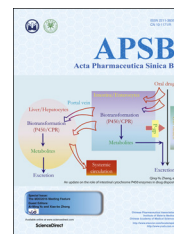
ORIGINAL ARTICLE

Tissue distribution and tumor uptake of folate receptor–targeted epothilone folate conjugate, BMS-753493, in CD2F1 mice after systemic administration

Hong Shen[a,†], Lifei Wang[a,†], Weiqi Chen[a], Krista Menard[b],
Yang Hong[c], Yuan Tian[c], Samuel J. Bonacorsi[c],
W. Griffith Humphreys[a], Francis Y. Lee[b], Jinping Gan[a,*]

[a]Pharmaceutical Candidate Optimization, Bristol-Myers Squibb Research & Development, Princeton, NJ 08543, USA
[b]Discovery Oncology, Bristol-Myers Squibb Research & Development, Princeton, NJ 08543, USA
[c]Chemistry, Bristol-Myers Squibb Research & Development, Princeton, NJ 08543, USA

Abstract   To assess targeting of an epothilone folate conjugate (BMS-753493) to the folate receptor (FR)-overexpressed tumor in mice bearing both FR+ and FR– tumors, a series of experiments were conducted by quantitative whole-body autoradiography (QWBA) and LC–MS/MS following i.v. administration of BMS-753493 or its active moiety, BMS-748285 in mice bearing FR+ (98M109) and FR– (M109) tumors. QWBA showed [^{3}H]BMS-753493–derived radioactivity was extensively distributed to various tissues. The FR over-expressing 98M109 tumors showed consistently higher level of radioactivity than FR-negative tumors (i.e., M109 tumors) up to 48 h post dose of [^{3}H]BMS-753493, despite the magnitude of difference between the tumors is relatively small (generally 3~5-fold). The radioactivity level in 98M109 tumors was 2~12-fold of normal tissues except intestine/content at 48 h post dose. No selective radioactivity uptake into 98M109 tumors over M109 or normal tissues was observed after i.v. administration of the active epothilone, [^{3}H]BMS-748285. LC–MS/MS measurements demonstrated that the concentrations of BMS-748285, presumably from hydrolysis of the folate conjugate, in 98M109 tumors were greater than those in M109 tumors after i.v. administration of BMS-753493 (2–3-fold) whereas no differential uptake in the tumors following BMS-748285 administration. Those data were consistent with radioactivity determinations. Those results demonstrated that the folate conjugation in BMS-753493 enabled moderately preferential distribution of the active epothilone to FR over-expressing 98M109 tumors, thereby supporting targeted delivery of cytotoxics through the folate receptor.

1. Introduction

Folic acid (folate, vitamin B9) is an essential nutrient that is involved in many metabolic pathways, including amino acid interconversions and nucleotide synthesis in normal and proliferating cells[1]. Folate receptor (FR), a family of glycosylphosphatidylinositol-linked proteins, captures folate and other ligands from the extracellular milieu and transports them inside the cell *via* a non-destructive, recycling endosomal pathway. Two membrane folate receptors (FRα and FRβ) and two soluble receptors (FRγ and FRδ) have been identified. Both FRα and FRβ are functional for high-affinity folate binding, although they can display some differences in their binding affinity for reduced folate cofactors or antifolates[2,3]. Surprisingly, FR is expressed on few cell types. FRα is detected on the apical surfaces of several epithelial cells where it is inaccessible to parenterally administered folate conjugates. FRβ, in contrast, is expressed on activated macrophages. FRγ and FRδ have been difficult to detect in human tissues[3–6].

Elevated expression of FRα occurs in many human malignancies, as in the case of ovarian, endometrial, renal, lung and breast carcinomas, especially when associated with aggressively growing cancers[2]. Non-mucinous ovarian cancer, which represents the majority of ovarian cancers, was the first tumor type to be associated with FR "over-expression"[7,8]. Importantly, conjugation of molecules to folic acid does not normally interfere with the high affinity ($K_d < 1$ nmol/L) of folate for its receptor nor with its endocytosis into cells[9]. Folate conjugates undergo internalization *via* receptor-mediated endocytosis, delivering the folate-linked drugs with high affinity into the cell interior, and with a proper linker, the active drug can be released under the acidic condition in the endosome[10,11]. Taken together, FR-targeted strategies could have a significant impact on cancer treatment for patients diagnosed with FR-positive (FR+) disease.

BMS-753493 is a novel epothilone folate conjugate which is designed to target FR over-expressing tumors. As shown in Fig. 1, a molecule of BMS-753493 contains an active epothilone, BMS-748285, a folate moiety, and a peptide linker with a disulfide bond tethering the epothilone piece. The mechanism of action of the epothilone folate conjugate is presumably through tight binding of the folate moiety to FRα receptor on the target cell surface, followed by endocytosis of the receptor–ligand complex, and subsequent cleavage of the linker to release the active epothilone. BMS-753493 demonstrated antitumor activity in various experimental mouse xenograft models where folate receptor was over-expressed[12]. By targeting the folate receptor, BMS-753493 is expected to provide preferential distribution of BMS-748285 into the FR+ tumors in comparison with FR negative (FR–) tumors or normal tissues, thereby improving the therapeutic index of cancer treatment. However, tissue distribution and tumor concentration of BMS-753493 and BMS-748285 relative to plasma and other normal tissue concentrations are unknown.

The goal of this study was to investigate the distribution of radioactivity after a single i.v. injection of [^{3}H]BMS-753493 and [^{3}H]BMS-748285 at molar equivalent doses to CD2F1 mice bearing bilateral subcutaneous murine lung tumors 98M109 (FR+) and M109 (FR–) at left or right flank of animal using quantitative whole body autoradiography (QWBA). Further experiments were performed to measure BMS-748285 levels in plasma, tumors, and representative normal tissue samples using LC–MS/MS assays after administration of unlabeled BMS-753493 and BMS-748285.

2. Materials and methods

2.1. Chemicals

[^{3}H]BMS-753493 (20.5Ci/mmol) and [^{3}H]BMS-748285 (21.3Ci/mmol) were supplied by Radiochemistry Group of Department of Chemical Synthesis, Bristol-Myers Squibb (Princeton, NJ, USA). Radiochemical purity of the compounds was determined to be > 99% by radio-HPLC. The chemical structures of BMS-753493 and BMS-748285 are shown in Fig. 1. Unlabeled BMS-753493 and BMS-748285 were supplied by the Process Research and Development, Bristol-Myers Squibb (New Brunswick, NJ, USA). All other chemicals were purchased from Sigma–Aldrich (St. Louis, MO, USA) unless stated in the text.

2.2. Cell culture

Folate receptor-positive Madison 109 (98M109) lung carcinoma cells were cultured in folate-deficient RPMI 1640 medium with 10% fetus bovine serum at 37 °C in a 5% CO_2 humidified atmosphere. Folate receptor negative Madison 109 (M109 cells) were cultured in normal RPMI 1640 medium under similar conditions before inoculation.

2.3. Animal models and tumors

Six- to eight-week old CD2F1 female mice were used in these studies. Mice were purchased from Harlan Sprague Dawley, Inc. (Indianapolis, IN, USA) and maintained in a specific pathogen free facility at Bristol-Myers Squibb Research and Development with food and water *ad libitum*. All animal experiments were done under a protocol approved by the Bristol-Myers Squibb Animal Care and Use Committee.

A tumor brei (2%, *w/v*) of M109 and 98M109 tumor cells were inoculated in the subcutaneous space of the mouse right and left flank of CD2F1 mice, respectively. High expression of FRα in 98M109 cells has been detected and confirmed (unpublished data). The xenografts were allowed to grow for two weeks after inoculation before being used in these distribution experiments. The approximate size of each tumor was around 100 mg at the time of dosing.

2.4. Tissue distribution study of radiolabeled BMS-753493 and BMS-748285

[^{3}H]BMS-753493 or [^{3}H]BMS-748285 was administered intravenously though tail vein injection at a dose level of 2.2 nmol/kg (4 and 1.2 mg/kg for BMS-753493 and BMS-748285, respectively; 10 mCi/kg) into M109 and 98M109 tumor-bearing mice for biodistribution experiments ($n=4$ in each treatment). The

*Corresponding author at: Pharmaceutical Candidate Optimization, Bristol-Myers Squibb, PO BOX 4000, Princeton, NJ 08543-4000, USA. Tel.: +1 609 252 7785; fax: +1 609 252 6802.

E-mail address: jinping.gan@bms.com (Jinping Gan).

†These authors made equal contributions to this work.
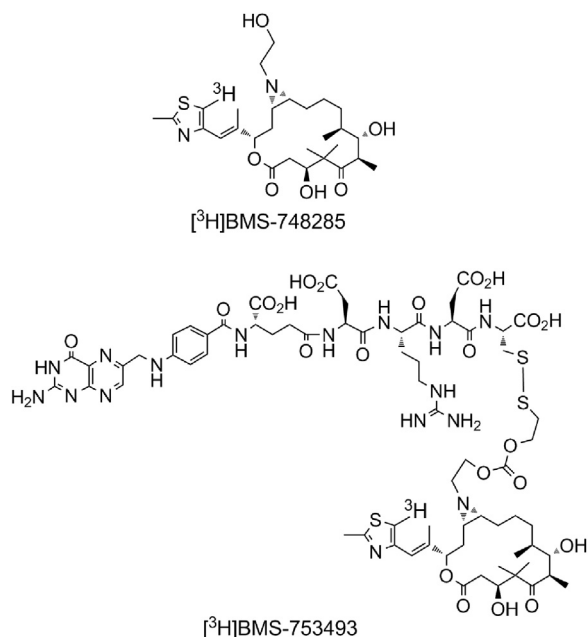
Figure 1 Chemical structures of [³H]BMS-753493 and [³H]BMS-748285.

maximum tolerated dose is 2.2 nmol/kg in mice for BMS-748285. Both agents were efficacious in 98M109 tumors at this dose. [³H]BMS-753493 dosing solution was freshly prepared in Delbecco's phosphate saline buffer just prior to dosing, and [³H]BMS-748285 solution was prepared freshly in a vehicle of cremphor:ethanol:5% dextrose water (1:1:8, v/v/v). One animal from each treatment was euthanatized at 0.5, 2, 24, and 48 h post-dose and immediately frozen in a dry ice-hexane bath (–70 °C) for 10 min. The distribution of radioactivity in animal at various times was determined by quantitative whole-body autoradiography as described as following.

2.5. Quantitative whole-body autoradiography (QWBA)

The frozen carcasses were rapidly stored below –20 °C until embedment in an ice-cold solution of 2% carboxymethylcellulose with a microtome stage. They were then frozen in a dry ice–hexane bath at –70 °C for approximately 60 min, followed by an overnight at –20 °C. Whole-body sections were obtained in a Leica CM3600 crymicrotome (Leica microsystems, Nussloch, Germany) at 40 μm thick in the sagittal plane. Sections were captured on adhesive tape (Scotch Tape No. 8210, 3M Ltd., St. Paul, MN, USA) at –20 °C. Sections at various levels were collected to include the major tissues and tumor, and then were dried in the cryomicrotome at –20 °C for 48 h. The sections of each animal was mounted on a cardboard, covered with a thin plastic wrap, and exposed along with calibration ³H-standards (range from 0.04 to 13 nCi/mg) to a ³H-sensitive phosphor imaging plate (Fuji Biomedical, Stamford, CT, USA) in light-tight exposure cassettes for 3 weeks at room temperature in a lead shielding box. After exposure, the imaging plates were scanned using Fuji 3000 image acquisition system (Fuji Biomedical). The image files were processed using MCID™ image analysis software (v.7.0, Imaging Research, Inc., St. Catherines, Ontario, Canada) and a standard curve was constructed from the integrated response and the radioactivity concentrations of the

[³H]-calibration standards. The concentrations of radioactivity were expressed as the μg equivalents of parent compound per gram sample (μg eq/g). A lower limit of quantification (LLQ) was applied to the data. The LLOQ were determined by using the radioactive concentration of background without tissues.

### 2.6. Tissue distribution and pharmacokinetics study of unlabeled BMS-753493 and BMS-748285

BMS-753493 or BMS-748285 was administered intravenously though tail vein injection at a dose level of 2.2 nmol/kg (4 and 1.2 mg/kg for BMS-753493 and BMS-748285, respectively) into the tumor-bearing CD2F1 mice (n=9 in each treatment; n=3 at each time point). BMS-753493 and BMS-748285 dosing solutions were prepared as described in the previous section. The blood samples were collected at 2, 6, and 24 h post dose by direct cardiac puncture using vacutainers containing K_3EDTA as an anticoagulant and 250 mmol/L phenylmethylsulphonylfluoride (PMSF)/methyl acrylate (1:1, v/v) as an stabilizer cocktail. The volume ratio of stabilizer cocktail versus blood was 1:50. Blood was centrifuged at 2000 × g for 5 min at 4 °C to obtain plasma, which was frozen immediately and stored at –20 °C until analyzed. Kidney, heart, and tumor tissue samples were collected and weighed, and were then frozen and stored at –70 °C until LC–MS/MS analysis.

2.7. Determination of test compounds by LC–MS/MS

The concentration of test compounds in plasma, heart, kidney, and tumors were determined by LC–MS/MS, as described as below.

2.7.1. Plasma
Plasma samples (50 μL) were mixed well with appropriate amounts of internal standard working solution containing [¹³C₂D₄]BMS-753493 and [¹³C₂D₄]BMS-748285 in methanol in a 96-well Sirocco protein precipitation polypropylene plate (Waters, Milford, MA, USA). The plates were centrifuged at 2000 × g for 12 min at room temperature, and 20 μL filtrate was injected for LC–MS/MS analysis.

2.7.2. Heart, kidney and tumor samples
Heart, kidney, or tumors were transferred separately to test tubes, cut into small pieces using a scissors, and then homogenized in phosphate buffered saline (PBS) solution containing 3.3 mmol/L of PMSF in a ratio of 1:3 (w/v). Each homogenate (50 μL) was mixed well with 100 μL of internal standard working solution containing [¹³C₂D₄]BMS-753493 and [¹³C₂D₄] BMS-748285 in methanol into a 96-well Sirocco protein precipitation polypropylene plate. The plate was centrifuged at 2000 × g for 12 min at room temperature, and 20 μL each filtrate was injected for LC–MS/MS analysis.

2.7.3. LC–MS/MS analysis
LC–MS analysis of BMS-753493, BMS-748285, and their internal standards was performed on a Sciex API 4000 mass spectrometer (Applied Biosystems, Foster City, CA, USA). High performance liquid chromatography (HPLC) consisted of three Shimadzu LC-10AD pumps with a SCL-10AVP system controller (Tokyo, Japan) and a CTC Analytics HTS PAL autosampler equipped with a cooling stack maintained at 5 °C (LEAP, Carrboro, NC, USA). The column used was a Luna C18(2) (2.0 mm × 50 mm,

3 μm, Phenomenex, Torrance, CA, USA) maintained at ambient temperature. Mobile phase A was water containing 10 mmol/L ammonium formate and 1.0% formic acid. Mobile phase B was 10 mmol/L ammonium formate and 1.0% formic acid in acetonitrile:water (90:10, *v/v*). HPLC flow rate was 0.3 mL/min and a linear gradient was run from 15% B at 0 min to 70% B at 2 min, held for 1 min and ramped back to 15% in 0.1 min. The total run time was 4 min. For each run, the flow from 1.2 to 2.2 min was delivered to the mass spectrometer. The rest was diverted to waste while a make-up flow consisting of 10 mmol/L ammonium formate and 1.0% formic acid in 11:9 (*v/v*) water: acetonitrile was delivered to mass spectrometer with a flow rate of 0.3 mL/min. The HPLC was interfaced with an API 4000 mass spectrometer equipped with an electrospray ionization source in the positive ion mode. The Turbospray probe temperature was 500 °C and the spray voltage was 4000 V. Ultra high purity nitrogen was used as the Gas 1, Gas 2, curtain gas and collision gas at flow rates of 30, 60, 30 and 12 (arbitrary unit), respectively. Multiple reactions monitoring (MRM) was used for detection. For BMS-753493 and its internal standard, the parent ions were the doubly charged ion $[M+2H]^{2+}$. The MRM transitions for BMS-753493 and BMS-748285 were m/z 785.3 to m/z 295.1 and m/z 537.3 to m/z 349.2, respectively. The MRM transitions for internal standard $[^{13}C_2D_4]$BMS-753493 and $[^{13}C_2D_4]$BMS-748285 were m/z 788.3 to m/z 295.1 and m/z 543.0.3 to m/z 355.0, respectively. The linear ranges were 1–500 and 10–5000 ng/mL, respectively, for BMS-748285 and BMS-753493.

2.8. Statistical analysis

Paired Student's *t*-test was used for comparison of mean cold BMS-748285 levels in various tumors and tissues.

3. Results

3.1. QWBA after administration of [³H]BMS-753493

The radioactivity was well visualized and quantified by whole body autoradiography in the tumor-bearing mice. Fig. 2 presents the quantitative tissue distribution of radioactivity from [³H]BMS-753493 at 48 h after i.v. administration of [³H]BMS-753493. In addition to tumors, [³H]BMS-753493-derived radioactivity was extensively distributed in a large variety of normal tissues with the highest concentrations in the gastrointestinal tract/content, liver, kidney, heart and bone marrow. Very little radioactivity was observed in the brain and spinal cord (Fig. 2 and Table 1). Interestingly, most of the radioactivity in the tumors was observed in the peripheral region and essentially no radioactivity in the core of tumors, indicating that the drug was not well perfused in the tumors (Fig. 3). Because of the heterogeneous distribution, the radioactivity in tumors was calculated from the peripheral region only.

The uptake into the FR overexpressing tumor 98M109 was greater than that in M109 tumors at all time intervals despite of only 3.4- to 4.5-fold difference in radioactivity from [³H]BMS-753493 observed (Fig. 3 and Table 1). The radioactivity of 98M109 tumor tissues was well retained through 48 h after [³H]BMS-753493 administration whereas that of normal tissues dropped quickly (Table 1), resulting in 2- to 12-fold higher [³H]BMS-753493 radioactivity in FR+ tumors compared to normal tissues except intestine/content at 48 h post dose (Table 1).
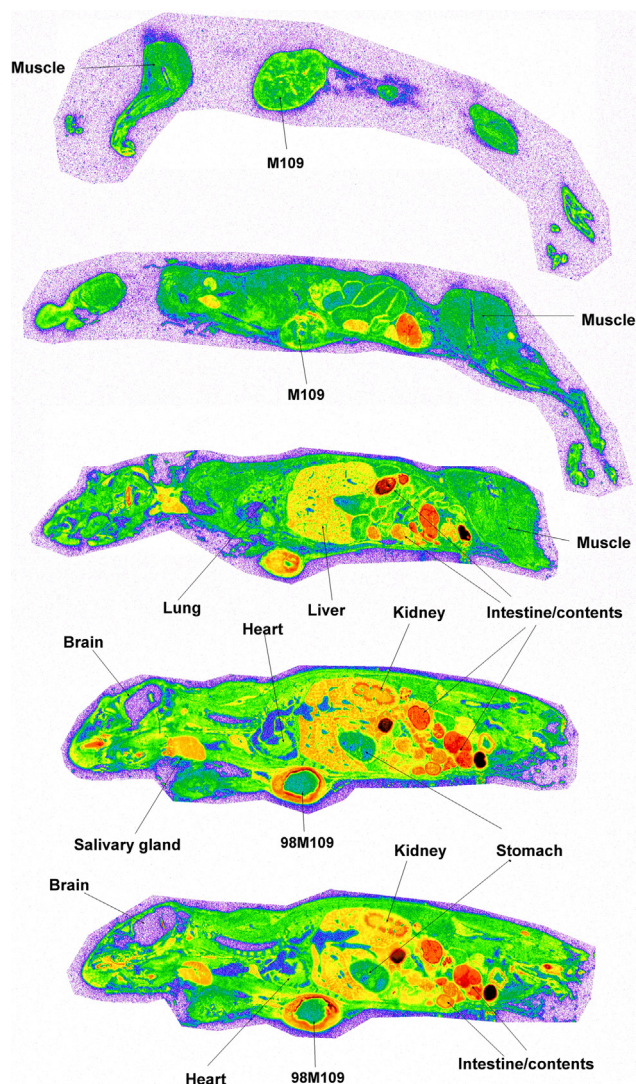
Figure 2 Autoradiograms of selected sections of mice at 48 h after dosing with [³H]BMS-753493. The representative whole-body autoradiograms of tumor-bearing mice following i.v. dose (2.2 nmol/kg or 4 mg/kg) of [³H]BMS-753493 at 48 h. The sections were to compare radioactivity distribution in M109 (FR–, right side) and 98M109 (FR+, left side) tumors, and selected tissues. Details of whole-body autoradiography are described in the Section of Materials and methods.

3.2. QWBA after administration of [³H]BMS-748285

Similarly, [³H]BMS-748285-derived radioactivity was extensively distributed following i.v. administration of [³H]BMS-748285. The tissues that had the highest radioactivity were the intestinal tract/content, liver, kidney, heart, bone marrow and tumors. Very little radioactivity was observed in the brain and spinal cord (Fig. 4 and Table 1). Likewise, heterogeneous distribution of [³H]BMS-748285 derived radioactivity was observed in both FR+ and FR– tumor tissues, indicating that the drug was not well perfused in the tumors (Fig. 3). In contrast to [³H]BMS-753493 observation, no differential distribution of [³H]BMS-748285 radioactivity into 98M109 *versus* M109 tumors (< 2.3-fold, Table 1). Therefore, no preferential targeting of [³H]BMS-748285 into the FR+ tumors relative to FR– tumors observed. However, [³H]BMS-748285-derived radioactivity in

Table 1   Radioactivity determined by QWBA in tumors and major mouse tissues after i.v. administration of [³H]BMS-753493 and [³H]BMS-748285 to the tumor-bearing mice.

Radioactivity in tissue (µg-eq. per gram tissue)

Tissue	[³H]BMS-753493 administration				[³H]BMS-748285 administration			
	0.5 h	2 h	24 h	48 h	0.5 h	2 h	24 h	48 h
M109 (FR−) tumor	1.7±0.6	1.2±0.4	1.2±0.7	0.5±0.1	3.3±1.0	2.3±0.5	1.6±0.7	1.4±0.3
98M109 (FR+) tumor	6.0±1.4	NC	4.1±2.2	2.3±1.1	6.3±1.5	4.7±1.3	2.4±0.9	3.3±0.7
Brain	0.1±0.0	LLQ	LLQ	LLQ	0.2±0.2	0.1±0.0	0.1±0.0	0.1±0.0
Blood	4.1±0.5	0.4±0.1	LLQ	LLQ	0.6±0.2	0.2±0.0	0.1±0.0	LLQ
Bone marrow	2.3±0.6	1.7±0.2	0.9±0.2	0.4±0.1	7.8±0.9	5.8±1.1	1.9±0.4	1.1±0.2
Heart	5.6±0.6	2.4±0.1	0.9±0.2	0.6±0.1	4.4±0.9	2.9±0.7	1.2±0.1	0.9±0.1
Liver	8.5±1.4	4.1±0.5	1.4±0.2	1.1±0.2	5.7±1.2	3.3±0.6	2.5±0.5	1.5±0.3
Lung	9.3±1.2	2.4±0.5	0.8±0.1	0.4±0.1	6.7±2.1	5.2±0.8	1.6±0.2	1.0±0.2
Kidney	11.3±4.5	6.0±3.0	1.5±0.3	1.4±0.4	8.6±1.7	4.8±0.7	2.9±0.6	1.4±0.4
Muscle	0.8±0.4	0.3±0.1	0.4±0.1	0.2±0.1	1.9±0.4	1.3±0.2	0.7±0.1	0.6±0.1
Skin	4.1±1.0	0.8±0.1	0.4±0.1	0.4±0.1	1.5±0.2	2.3±0.3	0.5±0.1	0.6±0.1
Salivary gland	3.1±0.5	3.1±0.6	1.9±0.3	1.4±0.2	7.5±0.9	5.8±0.9	3.1±0.3	2.5±0.4
Spinal cord	0.2±0.0	0.1±0.0	LLQ	LLQ	0.2±0.1	0.1±0.1	0.1±0.0	0.1±0.0
Intestine contents	52.6±21.7	45.8±32.3	37.0±26.5	4.7±2.7	49.4±26.2	49.9±29.0	28.8±26.6	10.2±8.4

NC: sample not collected due to missed tissue slicing; LLQ: below lower limit of quantitation.
Data are shown as mean ± SD.
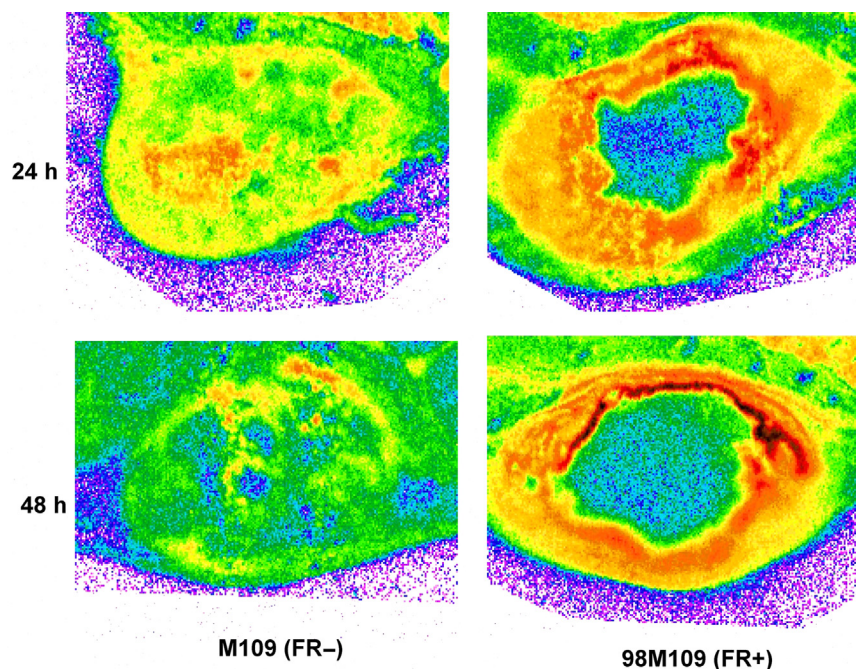
Figure 3   Autoradiograms of tumors after dosing with [³H]BMS-753493. The representative autoradiograms of tumor following i.v. doses (2.2 nmol/kg or 4 mg/kg) of [³H]BMS-753493 to tumor-bearing mice at 24 and 48 h. The sections were to compare radioactivity distribution in M109 (FR−) and 98M109 (FR+) tumors. Details of whole-body autoradiography are described in the Section of Materials and methods.

98M109 tumors did not differ to [³H]BMS-748285-derived radioactivity in the M109 tumors.

3.3.   Pharmacokinetics and tissue distribution after intravenous dosing of unlabeled BMS-753493 and BMS-748285

BMS-753493 was cleared rapidly from circulation, and it was detected in plasma at 2 h but not later time points after i.v.

injection of the drug. In contrast to BMS-753493, BMS-748285 converted from the conjugate was detectable through 24 h post dose (Fig. 5). The plasma levels of BMS-748285 after i.v. administration of BMS-753493 were significantly less than those after i.v. administration of the equal molar BMS-748285 (AUC of BMS-748285: 245.9 and 645.1 ng·h/mL, C_{24-h}: 3.2 and 13.5 ng/mL; Tables 2 and 3).

The concentrations of BMS-748285 in the tumors, heart and kidney were measured by LC–MS/MS. The levels of BMS-
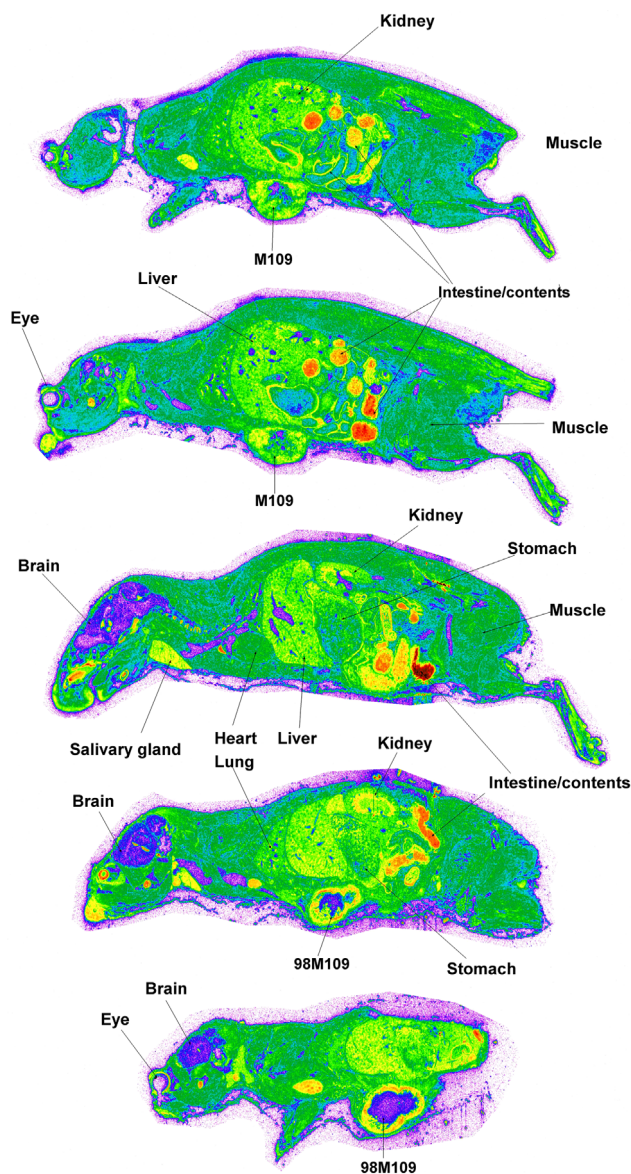
Figure 4 Autoradiograms of selected sections of mice at 48 h after dosing with [³H]BMS-748285. The representative whole-body autoradiograms of tumor-bearing mice following i.v. dose (2.2 nmol/kg or 1.2 mg/kg) of [³H]BMS-748285 at 48 h. The sections were to compare radioactivity distribution in M109 (FR–, right side) and 98M109 (FR+, left side) tumors, and selected tissues. Details of whole-body autoradiography are described in the Section of Materials and methods.

748285 in 98M109 tumors were 2.0- to 3.0-fold greater than those in M109 tumors after i.v. administration of BMS-753493 while no difference in BMS-748285 levels between the tumors after administration of BMS-748285 (<1.2-fold, Table 2). However, BMS-748285 concentrations of 98M109 tumors following i.v. administration of BMS-753493 were similar to those of M109 following i.v. administration of BMS-748285. The concentrations of BMS-748285 in the kidney and heart, two vital organs, following i.v. administration of BMS-753493 are significantly less than those after i.v. dosing of BMS-748285 (Fig. 6). The tissue concentrations of BMS-753493 was not detectable in all tissue samples after dosing of BMS-753493.
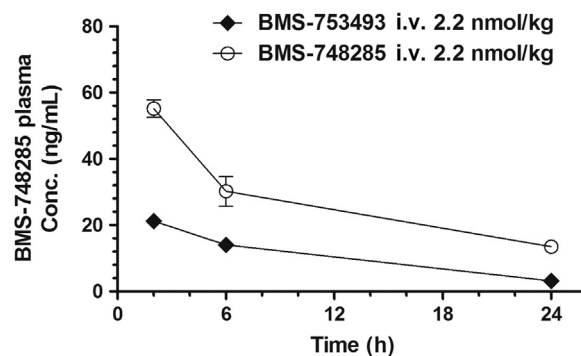
Figure 5 Concentration *versus* time profile of BMS-748285 in mouse plasma after i.v. administration of 2.2 nmol/kg BMS-753493 or BMS-748285.

4. Discussion

One of the greatest challenges of anti-cancer treatment involves the delivery of therapeutically active levels of drug to tumors while not eliciting toxicity in non-tumor tissue. Selective drug targeting has long been a goal of drug development and there have been numerous investigations aimed at developing more efficient systems for the site specific delivery of drugs. This strategy has recently garnered great excitement in the oncology community with impressive clinical benefits reported on antibody directed cytotoxic drugs including T-DM1 and SGN-35[13–15]. There were also considerable efforts to take advantage of specific folate receptors on the cancer cell surface by conjugation of folate with highly potent anti-cancer drugs for efficient delivery[5,16]. 99Tc-EC20, a folate-targeted imaging agent, is in development for the diagnosis and identification of patients with FR+ tumors[17]. Clinical study involving greater than 100 patients indicated that there is marked selective uptake of 99Tc-EC20 in ovarian, renal, and pituitary tumors, reflecting the potential for therapeutic response through folate-targeted therapy[18]. The clinical proof-of-concept for FR-targeted efficacy of EC145, a conjugate of folic acid and desacetylvinblastine hydrazide, has been reported recently[19]. EC145 and pegylated liposomal doxorubicin (PLD) showed a statistically significant delay in progression-free survival over standard therapy in women with platinum-resistant ovarian cancer.

BMS-753493 contains a folate moiety and a potent epothilone analog, BMS-748285, attached through a peptide linker. It is designed to enable tumor-specific delivery of the highly cytotoxic epothilone analog BMS-748285 to its site of action, resulting in the blockade of cells in mitosis and eventual cell death. The choice of the epothilone as "cytotoxic warhead" in the target-delivery approach is considered ideal because the mechanism of action of epothilones (microtubule stabilization) is validated as capable of producing clinical benefits[20–22]. In addition, the selective cytotoxicity of epothilones against proliferating relative to non-proliferating cells (except neurons) reduces the likelihood of receptor-mediated normal tissue toxicity in those tissues that do express FR. Lack of FR expression in neurons reduces the likelihood of neuropathy, which is a key dose-limiting toxicity specific to this class of cytotoxic agents[23,24]. Finally, the molecular potency of BMS-748285 ($IC_{50} < 1$ nmol/L) maximizes the potential to effect cell kill with the delivery of a limited number of drug molecules[12].

In this study, we demonstrated modestly selective uptake and retention of BMS-753493 and BMS-748285 in FR-postive 98M109 tumors over FR-negative M109 tumors and normal tissues after administration of the folate-epothilone conjugate. This conclusion

Table 2 BMS-748285 concentrations determined by LC–MS/MS in tumors, kidney, and heart after i.v. administration of BMS-753493 or BMS-748285 to the tumor-bearing mice.

		BMS-748285 concentration				
Treatment	Time (h)	Plasma (ng/mL)	M109 tumor (FR−) (µg/g tissue)	98M109 tumor (FR+) (µg/g tissue)	Kidney (µg/g tissue)	Heart (µg/g tissue)
BMS-753493	2	21.2 ± 2.5	0.10 ± 0.03	0.30 ± 0.10	1.73 ± 0.15	0.17 ± 0.04
	6	14.0 ± 3.0	0.16 ± 0.01	0.35 ± 0.05	1.22 ± 0.12	0.18 ± 0.03
	24	3.2 ± 0.4	0.09 ± 0.01	0.18 ± 0.07	0.41 ± 0.05	0.11 ± 0.02
BMS-748285	2	55.2 ± 4.7	0.25 ± 0.02	0.29 ± 0.11	3.36 ± 0.09	0.93 ± 0.13
	6	30.2 ± 7.7	0.26 ± 0.07	0.27 ± 0.05	2.63 ± 0.13	0.61 ± 0.17
	24	13.5 ± 2.0	0.24 ± 0.02	0.24 ± 0.03	1.38 ± 0.04	0.33 ± 0.07

Data are shown as mean ± SD.

Table 3 Conversion of BMS-753493 to BMS-748285 in plasma of mice dosed IV with BMS-753493 or BMS-748285.

i.v. Dose	BMS-753493 (MW 1569.7)	BMS-748285 (MW 536.7)
Dose (mg/kg)	4.0	1.2
Dose (µmol/kg)	2.55	2.24
AUC of BMS-748285 (ng·h/mL)[a]	245.9 ± 36.1	645.1 ± 82.6
Exposure of BMS-748285 (%)[b]	33%	NC

[a]Area under the curve (AUC) was calculated based on simple trapezoidal rule in excel.
[b]Exposure of BMS-748285 was estimated by comparing the AUC values of BMS-748285 in plasma after dosing of BMS-753493 with that after dosing of BMS-748285.

was based on (1) [3H]BMS-753493 radioactivity concentrations in 98M109 tumors being higher than those in M109 tumors after administration of [3H]BMS-753493, and no difference observed in the radioactivity between 98M109 and M109 tumors following [3H]BMS-748285 dosing; (2) BMS-748285 concentrations in 98M109 tumor tissue being significantly greater than those in M109 following administration of unlabeled BMS-953493 but not BMS-748285; and (3) heart and liver, two vital normal organs, displaying lower levels of BMS-748285 when BMS-753493 was injected compared with equal molar BMS-748285 administration. Based on these facts, we hypothesize the folate receptor over-expressed on the surface of cancer cells enable selective uptake of the epothilone folate conjugate, BMS-753493, into FR-positive tumors. Therefore, BMS-753493 may have improved safety margin over the unconjugated epothilone BMS-748285. However, the folate epothilone conjugate does not appear to markedly enhance delivery to FR-positive tumors compared to the epothilone itself.

QWBA studies showed that the radioactivity derived from either [3H]BMS-753493 or [3H]BMS-748285 in mice was extensively distributed to a large variety of tissues. In addition to tumor cells, the high levels of BMS-753493 and BMS-748285 radioactivity was detected in gastrointestinal tract and content, liver, kidney, heart and bone marrow (Figs. 2 and 4, Table 1). The highest radioactivity concentrations in those tissues were observed at 0.5 h post dose. BMS-748285 has high lipophilic property, which allows rapid penetration into tissues. The wide tissue distribution of [3H]BMS-753493 derived radioactivity may reflect the nonspecific release of active epothilone after disulfide exchange in plasma. The steady-state volume distribution

(V_{dss}) values of BMS-753493 were small when tested across preclinical species whereas BMS-748285 has large V_{dss} (data on file but not shown). Autoradiograms showed that radioactivity in the center area of tumors were lower than that in the edge area of tumors (Fig. 3). This is most likely due to lack of tumor vascularization and blood supply in the center region.

QWBA studies showed that [3H]BMS-753493 derived radioactivity was well retained in FR over-expressing tumors versus FR-negative tumors. Consistently, LC–MS/MS experiments demonstrated that the levels of BMS-748285 in 98M109 tumors were greater than those in M109 after administration of BMS-753493 (Table 2). The tumor concentrations of drug related radioactivity as listed in Table 1 were higher than the BMS-748285 levels in 98M109 tumors when measured by LC-MS assay (Table 2), although the radioactivity was predominantly BMS-748285 related. This can be explained by a difference in methodology; only the peripheral region of tumor tissue was used to calculate the radioactivity concentration in QWBA due to heterogeneity observed in tumor radioactivity distribution whereas the whole tumor tissue was homogenized for LC–MS/MS analysis. These observations support the involvement of folate receptor in the tumor uptake of the epothilone after dosing of the epothilone folate conjugate, and such preferential delivery is likely a result of folate receptor expression differences rather than of physiological or histological differences among the tumors and normal tissues.

The tissue distribution of BMS-753493 and BMS-748285 may be affected by ATP-binding cassette (ABC) efflux transporters such as P-glycoprotein (P-gp). Radioactivity of [3H]BMS-753493 and [3H]BMS-748285 in the brain was lower as compared to blood and other tissues, even below the detection level at certain time points, indicating very poor penetration into brain despite both compounds showing wide distribution into other normal tissues. In a different study, we found out that both BMS-753493 and BMS-748285 were substrates for P-gp using human MDR1 transfected cell models and P-gp knockout mice (unpublished data).

Although preferential delivery to FR-positive tumors was demonstrated, the magnitude of selectivity versus FR-negative tumors was not very high (3- to 5-fold). We suspect the modest differential distribution was at least in part due to inadequate linker technology. The disulfide bond readily reacts with cellular and circulating thiol pool including cysteine, glutathione, and free thiols in plasma including cysteine-34 of serum albumin[25]. This disulfide exchange releases free epothilone BMS-748285. In fact, it was estimated that 33% of the epothilone conjugate was converted to BMS-748285 in circulation from the PK data (Table 3). The nonspecific cleavage in turn diminished the targeting specificity of the folate conjugate.
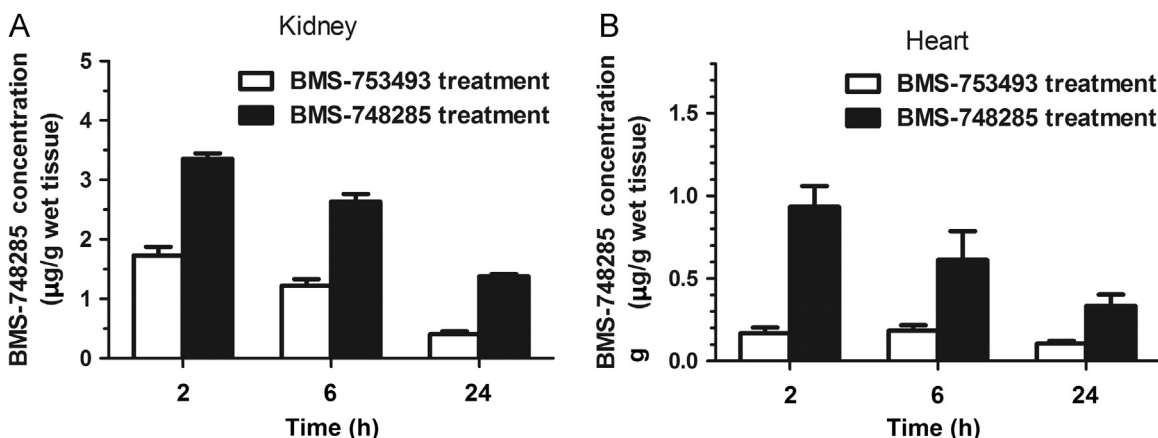
Figure 6 Concentrations of BMS-748285 in the kidney (A) and heart (B) after i.v. administration of 2.2 nmol/kg BMS-753493 or BMS-748285.

5. Conclusions

In summary, this study has demonstrated that BMS-753493, an epothilone folate conjugate, preferentially distributed the active epothilone into FR over-expressing 98M109 tumor over FR-negative tumors and tissues, compared to epothilone administration. The epothilone folate conjugate reduced systemic exposure to free epothilone and decreased cellular penetration into FR-negative tumors and tissues. The preferential distribution implies the folate conjugate might improve therapeutic margin in the treatment of tumors over-expressing folate receptors.

References

1. Clifford AJ, et al. The dynamics of folic acid metabolism in an adult given a small tracer dose of ^{14}C-folic acid. *Adv Exp Med Biol* 1998;**445**:239–51.
2. Low PS, Antony AC. Folate receptor-targeted drugs for cancer and inflammatory diseases. *Adv Drug Deliv Rev* 2004;**56**:1055–8.
3. Ross JF, Chaudhuri PK, Ratnam M. Differential regulation of folate receptor isoforms in normal and malignant tissues *in vivo* and in established cell lines. Physiologic and clinical implications. *Cancer* 1994;**73**:2432–43.
4. Low PS, Kularatne SA. Folate-targeted therapeutic and imaging agents for cancer. *Curr Opin Chem Biol* 2009;**13**:256–62.
5. Salazar MD, Ratnam M. The folate receptor: what does it promise in tissue-targeted therapeutics? *Cancer Metastasis Rev* 2007;**26**:141–52.
6. Weitman SD, Lark RH, Coney LR, Fort DW, Frasca V, Zurawski VR Jr, et al. Distribution of the folate receptor GP38 in normal and malignant cell lines and tissues. *Cancer Res* 1992;**52**:3396–401.
7. Campbell IG, Jones TA, Foulkes WD, Trowsdale J. Folate-binding protein is a marker for ovarian cancer. *Cancer Res* 1991;**51**:5329–38.
8. Toffoli G, Cernigoi C, Russo A, Gallo A, Bagnoli M, Boiocchi M. Overexpression of folate binding protein in ovarian cancers. *Int J Cancer* 1997;**74**:193–8.
9. Antony AC. The biological chemistry of folate receptors. *Blood* 1992;**79**:2807–20.
10. Kamen BA, Capdevila A. Receptor-mediated folate accumulation is regulated by the cellular folate content. *Proc Natl Acad Sci U S A* 1986;**83**:5983–7.
11. Leamon CP. Folate-targeted drug strategies for the treatment of cancer. *Curr Opin Investig Drugs* 2008;**9**:1277–86.
12. Covello K, Flefleh C, Menard K, Wiebesiek A, McGlinchey K, Wen M, et al. Preclinical pharmacology of epothilone-folate conjugate BMS-753493, a tumor-targeting agent selected for clinical development. San Diego: The 99th AACR Annual Meeting. *Cancer Res* 2008;**68**:S2326.
13. Junttila TT, Li G, Parsons K, Phillips GL, Sliwkowski MX. Trastuzumab-DM1 (T-DM1) retains all the mechanisms of action of trastuzumab and efficiently inhibits growth of lapatinib insensitive breast cancer. *Breast Cancer Res Treat* 2011;**128**:347–56.
14. Krop IE, Beeram M, Modi S, Jones SF, Holden SN, Yu W, et al. Phase I study of trastuzumab-DM1, an HER2 antibody–drug conjugate, given every 3 weeks to patients with HER2-positive metastatic breast cancer. *J Clin Oncol* 2010;**28**:2698–704.
15. Younes A, Bartlett NL, Leonard JP, Kennedy DA, Lynch CM, Sievers EL, et al. Brentuximab vedotin (SGN-35) for relapsed CD30-positive lymphomas. *N Engl J Med* 2010;**363**:1812–21.
16. Leamon CP, Low PS. Delivery of macromolecules into living cells: a method that exploits folate receptor endocytosis. *Proc Natl Acad Sci U S A* 1991;**88**:5572–6.
17. Fisher RE, Siegel BA, Edell SL, Oyesiku NM, Morgenstern DE, Messmann RA, et al. Exploratory study of 99mTc-EC20 imaging for identifying patients with folate receptor-positive solid tumors. *J Nucl Med* 2008;**49**:899–906.
18. Sega EI, Low PS. Tumor detection using folate receptor-targeted imaging agents. *Cancer Metastas Rev* 2008;**27**:655–64.
19. Naumann RW, Coleman RL, Burger RA, Sausville EA, Kutarska E, Ghamande SA, et al. PRECEDENT: a randomized phase II trial comparing vintafolide (EC145) and pegylated liposomal doxorubicin (PLD) in combination versus PLD alone in patients with platinum-resistant ovarian cancer. *J Clin Oncol* 2013;**31**:4400–6.
20. Cobham MV, Donovan D. Ixabepilone: a new treatment option for the management of taxane-resistant metastatic breast cancer. *Cancer Manag Res* 2009;**1**:69–77.
21. Frye DK. Advances in breast cancer treatment: the emerging role of ixabepilone. *Expert Rev Anticancer Ther* 2010;**10**:23–32.
22. Huang H, Menefee M, Edgerly M, Zhuang S, Kotz H, Poruchynsky M, et al. A phase II clinical trial of ixabepilone (Ixempra; BMS-247550; NSC 710428), an epothilone B analog, in patients with metastatic renal cell carcinoma. *Clin Cancer Res* 2010;**16**:1634–41.
23. Donovan D. Management of peripheral neuropathy caused by microtubule inhibitors. *Clin J Oncol Nurs* 2009;**13**:686–94.
24. Lee JJ, Swain SM. Peripheral neuropathy induced by microtubule-stabilizing agents. *J Clin Oncol* 2006;**24**:1633–42.
25. Kratz F, et al. Probing the cysteine-34 position of endogenous serum albumin with thiol-binding doxorubicin derivatives. Improved efficacy of an acid-sensitive doxorubicin derivative with specific albumin-binding properties compared to that of the parent compound. *J Med Chem* 2002;**45**:5523–33.